Chemisorption of Benzene on Pt(111), Pd(111), and Rh(111) Metal Surfaces: A Structural and Vibrational Comparison from First Principles

C. Morin,[†] D. Simon,[‡] and P. Sautet*,[†]

Laboratoire de Chimie, UMR CNRS 5182, Ecole Normale Supérieure de Lyon, 46 Allée d'Italie, F-69364 Lyon Cedex 07, France, and Laboratoire de Spectrométrie Ionique et Moléculaire (LASIM - CNRS UMR 5579), Université Claude Bernard - Lyon I, 43 Bd du 11 novembre 1918, F-69622 Villeurbanne Cedex, France

Received: November 4, 2003; In Final Form: January 9, 2004

The adsorption mode of aromatic molecules on transition metal surfaces has an important implication in their catalytic transformation. As platinum, palladium, and rhodium metals are some of the most employed in heterogeneous catalytic reactions, and benzene C_6H_6 is the smallest aromatic molecule, these systems are good models for understanding their interactions. Those are approached in this study by first-principles density functional periodic calculations on (111) metal surfaces. The energetic results show that benzene can adsorb predominantly in a bridge position on Pt(111), while on Pd(111) and Rh(111), benzene molecules on bridge and hollow positions have similar adsorption energies. These conclusions are confirmed by the comparison of vibrational spectra from experiment (HREELS) and simulation: most peaks of the spectra can be assigned with a bridge site molecule, but for each case some peaks or shoulders can be understood only if a fraction of hollow sites is supposed. The adsorption exothermicity increases from palladium to platinum and to rhodium. An electronic analysis, via the projected densities of states and the differential electron density isosurfaces, helps to understand how this interaction can be related to the shape and filling of the *d*-band. The adsorption process is described as a compromise between a destabilizing distortion of the molecule and surface, and a stabilizing interaction between them. Pd corresponds to weak distortion and interaction terms, while Rh and Pt are associated with large contributions.

I. Introduction

The catalytic conversion of aromatic molecules is a very important process in the chemical industry, both for environmental and economical reasons.[1,2] Hydrogenation or hydrogenolysis of these stable hydrocarbon molecules are the main target reactions in petroleum refining and reforming processes which are performed on transition metal catalysts. A strong incentive is provided by the recent European legislation, which has set a strict limit on the concentration of benzene and other aromatic molecules in fuels.[3] As a consequence, the bonding and coordination of aromatic compounds on transition metal surfaces continue to raise a large interest.

Benzene is a model compound for aromatic molecules, with a delocalized aromatic π electron system which participates directly in the bonding with the surface. The chemisorption of benzene has therefore been studied from several experimental and theoretical approaches. It is now clearly established that, at low coverage, the bonding of benzene is exclusively through the π electron system, resulting in a parallel or flat configuration on the close-packed transition metal surfaces.[4,5] The comparison of different metal surfaces, for the chemisorption or reactivity properties with respect to benzene, however, remains an important issue, to understand and optimize the catalytic performances. The main focus of the present paper is to give insight on how the interaction between benzene and a surface varies when the metal is changed among three group-8 transition metal atoms: Pt, Pd, and Rh. The approach will be limited to the close-packed, most stable, (111) surface of these metals.

Even if the basic aspects of benzene adsorption on transition metal surfaces are reasonably well understood, some important aspects, such as the preference for a particular adsorption site, the adsorption energy, or the general mechanism underlying the metal-surface interaction are however more difficult to extract from the experimental approaches, and are still the subject of an active debate. For example, the assignment of the adsorption sites from experimental techniques results in conflicting and unclear conclusions. The possibility in some cases of obtaining multiple occupation of adsorption sites makes the picture even more complex. One of the key techniques used to study benzene adsorption is vibrational spectroscopy. The adsorbate orientation can be easily obtained, but the determination of the adsorption site requires a detailed interpretation of the data.

First-principles calculations can bring additional and complementary insights to the problem. They especially provide information or analysis which cannot be easily extracted from experiments. Besides general energetic and structural results, they can yield an accurate simulation of some specific experimental information, such as vibrational frequencies or intensities.

The adsorption of benzene on Pt(111) has been studied in detail with a large number of experimental characterization techniques, including reflection−adsorption infrared spectroscopy (RAIRS),[6] high-resolution electron energy loss spectroscopy (HREELS),[7,8] low-energy electron diffraction (LEED),[9,10] and scanning tunneling microscopy (STM).[11−14] The RAIRS

* Corresponding author. E-mail: sautet@ens-lyon.fr. Telephone: (33) 4 72 72 81 55.

[†] Laboratoire de Chimie, UMR CNRS 5182, Ecole Normale Supérieure de Lyon.

[‡] Laboratoire de Spectrométrie Ionique et Moléculaire (LASIM - CNRS UMR 5579) Université Claude Bernard.

10.1021/jp0373503 CCC: $27.50
Published on Web 04/14/2004

vibrational spectrum was assigned to a simultaneous occupation of 3-fold and 2-fold sites.[6] The interpretation of thermal desorption spectroscopy (TDS) experiments also proposed that more than one chemisorption site is occupied, with a very low migration rate between these states.[15] This compares well with the local information provided by STM, which clearly shows that several chemisorption sites can be occupied at low coverage and low temperature on the surface.[11−13] However, LEED concludes only in a bridge site occupation, even in the case where benzene is coadsorbed with CO.[10,16] In the absence of CO, the situation is further complicated by the fact that the surface structure of benzene is disordered. Additionally, a STM study in solution at a coverage of 0.14 proposes a structure where only bridge sites are populated.[17] The near edge X-ray absorption fine structure (NEXAFS) results are even more contrasting, since they are interpreted in terms of atop adsorption of benzene, the center of mass of the molecule above a Pt surface atom,[18] while angle-resolved ultraviolet photoelectron spectroscopy (ARUPS) proposes a hollow site adsorption.[19] Hence, multiple conclusions arise from spectroscopic or microscopic techniques, and the resulting situation is quite confusing.

The situation is also rather complex on Rh(111). It is first difficult to clean the sample and to avoid contamination from residual CO in the gas phase. As a consequence, some early structures for benzene on Rh(111)[20] were later reanalyzed on the basis of a coadsorption with CO.[16] These coadsorption structures with CO have been studied with several techniques including HREELS, LEED, STM, and UPS. STM clearly suggests a 3-fold hollow site for the benzene molecule, as seen in the three-lobe image.[21,22] LEED and HREELS also indicate a hollow site,[16] but there is still a debate on the strength of the 3-fold Kekulé type distortion of the adsorbed molecule. Initial LEED analyses proposed a very strong 3-fold distortion, while more recent ones[23] gave a much more modest deformation. In contrast, ARUPS gives atop adsorption related to a C_{6v} symmetry at low coverage, switching to a 3-fold hollow site at high coverage, associated with a moderate distortion of the ring. If we now turn to the adsorption of benzene only (without coasdorbed CO), HREELS shows a mixture of bridge and hollow adsorption structures, the first one being dominant, while LEED, from the presence of a glide plane symmetry, is compatible with benzene molecules centered over bridge sites. This was elegantly interpreted as an ordered bridge site structure, with a small number of additional benzene molecules adsorbed at 3-fold hollow sites and disordered on the surface. STM in solution proposes that different ordered overlayers, with coverage only changing between 0.17 monolayer (ML) and 0.11 ML could be associated with a different binding site of the molecule, either 3-fold or 2-fold.[17] It was suggested, however, that a molecule from the solution could be coadsorbed with benzene on the low-coverage structure. Such an effect was not seen on Pt(111).

On the Pd(111) surface, the experimental data is not as abundant. A recent X-ray photoelectron spectroscopy (XPS) and NEXAFS analysis confirms that the molecule is chemisorbed flat at low coverage but suggests a strong tilt at high coverage.[24] It was proposed from HREELS that only one site is populated on the surface, and from a symmetry analysis that this site has a C_s symmetry.[25] In contrast, ARUPS gives a high-symmetry C_{6v} adsorption structure, attributed to a top site. It also shows that the energies of the upper-most molecular orbitals of benzene are shifted by 1.3−1.5 eV. For the coadsorption structure with CO, a 3-fold hollow site is determined by LEED, associated with a negligible Kekulé distortion.[23]

The adsorption of benzene on several transition metal surfaces has been theoretically studied with simple semiempirical methods, which can only provide general trends on the molecule−surface interaction.[26−28] First-principles computational methods have been applied to the chemisorption of benzene on Pt[1,29] and on Ni(111) surfaces.[30,31] To our knowledge, the adsorption on Rh and Pd surfaces has not been considered in detail from density functional theory approaches. It should be emphasized here that such first-principles studies of aromatic molecules on transition metal surface are complicated because of the large number of atoms in the surface unit required for a realistic simulation. On Pt(111), it was concluded from a comparison between experimental and calculated vibrational spectra that the bridge site is favored at low coverage, while the hollow site becomes preferred with increasing coverage.[1,29] The study has also been extended to molecular diffusion and hydrogenation.

In this paper, we present a comparative study of the chemisorption of benzene on three (111) transition metal surfaces: Pt, Pd, and Rh. The surfaces will be described by periodic slabs. The focus is on the adsorption site, mechanism, and vibrational properties, with a close comparison with experimental results. Results will also be compared with those recently obtained on Ni(111) with the same method. In section II, we describe the methods we used to perform calculations of total energies and vibrational spectra. The results for the adsorption of pure benzene on Pt, Pd, and Rh(111) surfaces, and for the coadsorption of benzene and CO on Rh(111) are presented in section III. We discuss our results in term of vibrational and electronic properties, through the analysis of projected densities of states and differential charge density images, in section IV.

II. Methods

The Vienna ab initio simulation package (VASP) code has been used for the calculations.[32,33] It solves the Kohn−Sham equations of density functional theory (DFT) using a plane-wave basis set. For this set, a cutoff energy of 400 eV was used. The electron−ion interaction was described with the projector augmented wave (PAW) method.[34] Exchange and correlation effects are treated in the generalized gradient approximation (GGA), in the formulation of Perdew-Wang-91.[35]

The supercell was chosen that corresponds to a p(3×3) superstructure of the adsorbed benzene molecules, giving a 1/9 monolayer coverage. This size of unit cell has been selected in order to avoid lateral interactions between nearest-neighbor molecules and hence to address the low- or medium-coverage situations. Indeed, an XPS study of benzene adsorption on Pd(111)[24] shows that for coverages higher than 1/6, benzene molecules interact, which results in the presence of two different adsorption configurations, one parallel to the surface and another one tilted, desorbing at ∼150 K. Brillouin-zone integrations have been performed using a $5 \times 5 \times 1$ Monkhorst-Pack grid[36] and a Methfessel-Paxton smearing[37] of 0.25 eV. In a previous study of the adsorption of benzene on Pt(111), it was shown that this density of points allows one to reach a reasonable convergence of the adsorption energy.[29] It also showed that a slab consisting of four layers of metal atoms for the surface was sufficient. This model has been chosen in the present study, with the two uppermost layers allowed to relax. The slab is repeated periodically in the direction perpendicular to the surface and the vacuum space between neighboring slabs was set to an equivalent of five layers of metal, i.e., more than 13 Å in each case.

The vibrational frequencies and corresponding eigen-modes have been calculated by the diagonalization of the Hessian matrix. This matrix has been evaluated analytically by calculating the forces $F^{B,\beta}_{A,\alpha}(\alpha = x,y,z)$ that are exerted on the A atom of the system due to an infinitesimal displacement of $d\beta_B$ of the β coordinate of the B atom. Then we approximated $\mathrm{Hess}^{B,\beta}_{A,\alpha} = d^2E/(d\alpha_A\, d\beta_B)$ by $\mathrm{Hess}^{B,\beta}_{A,\alpha} = (F^{B,\beta}_{A,\alpha} - F^{B,-\beta}_{A,\alpha})/2\delta\beta_B$, where $\delta\beta_B$ stands for a finite, but low displacement of the β coordinate of the B atom. The intensities of the simulated spectra are related to the squared dynamic dipole moment.[38,39] For the ith mode, $I_i \propto |d\mu/|d\eta_i||^2$ where $d\eta_i$ corresponds to an infinitesimal displacement of the different atoms of the system, according to the mode: $d\eta_i = \sum_{\alpha=x,y,z}\sum_{A=atom} C^i_{\alpha A}\sqrt{m_A}d\alpha_A$, with, for each mode i, $\sum_{\alpha,A}(C^i_{\alpha,A})^2 = 1$. We evaluated $d\mu/|d\eta_i|$ as the slope of the function $\mu(\theta) = \mu(r_0 + \theta\, d\eta_i)$, i.e., the variation of the dipole moment when the molecule moves from the equilibrium r_0 in the direction of the vibrational mode. When the energy losses are observed in the direction of the specular reflection, active modes for high-resolution electron energy loss spectroscopy (HREELS) belong to the totally symmetric A_1 representation of the symmetry point group.[7] So, the spectra are simulated by first taking this selection rule into account and selecting A_1 modes; the intensity of each active mode has then been computed from the squared dynamic dipole moment, and a Gaussian broadening of 18 cm^{-1} is applied in the graph.

III. Adsorption Sites for Each Metal Surface

As previously explored in the case of the adsorption of benzene on Pt(111),[29] several adsorption configurations, with high symmetry and with the aromatic ring parallel to the surface, have been taken into account as starting points for geometry optimization. Among the optimized benzene configurations on Pt, Pd and Rh(111), two different structures proved to be more stable than the others, shown in Figure 1. In the bri30 conformation, the benzene ring center is located in a bridge position above two metal atoms, with no C−H bond in the [110] direction. In the hcp0 conformation, the aromatic ring is in a 3-fold position, with two C−H bonds in the [110] direction. In each case, the other adsorption possibilities (bri0 and hcp30, see ref 29 for details) are less stable by at least 0.3 eV, while the top adsorptions are found unstable.

Table 1 and Table 2 show the adsorption energies of benzene on Pt(111), Pd(111), Rh(111), and Ni(111) surfaces, and the geometric characteristics on the bri30 and hcp0 positions, respectively. In the case of nickel, the calculations have been done previously by Mittendorfer et al.[30]

III.1. Benzene on Pt(111). As shown in ref 29, the bri30 conformation is found as the most stable one. The adsorption energy on such a configuration is $E_{ads} = -0.90$ eV, while on the hcp0 site, it is only −0.67 eV. This most favorable adsorption structure is confirmed by the analysis of the computed vibrational spectra and its comparison with the experimental HREELS ones.[7,8,16] Indeed, the experimental spectra show six well-resolved peaks at 360, 570, 830, 1130, 1410, and 3000 cm^{-1}, and two shoulders at 920 and 1310 cm^{-1}. The computed frequencies listed in Table 3 and the spectra of Figure 2 show how the bri30 structure allows one to reproduce and understand all measured bands, including qualitatively their relative intensity, except the shoulder at 1310 cm^{-1}, that can be explained by a low proportion estimated to ∼1/25th of hcp0 structure (see Table 4 and Figure 2) presenting in the calculation a ν_9 mode at 1345 cm^{-1}. The higher stability of the bri30 structure, however, does not completely agree with the experimental LEED conclusion. In the presence of coadsorbed CO, a bri30 configuration is shown to be adopted,[10] while for pure benzene[9] a bri0 (as bri30 in Figure 1, but rotated by 30°) position, in a highly distorted geometry is proposed from a delicate diffuse

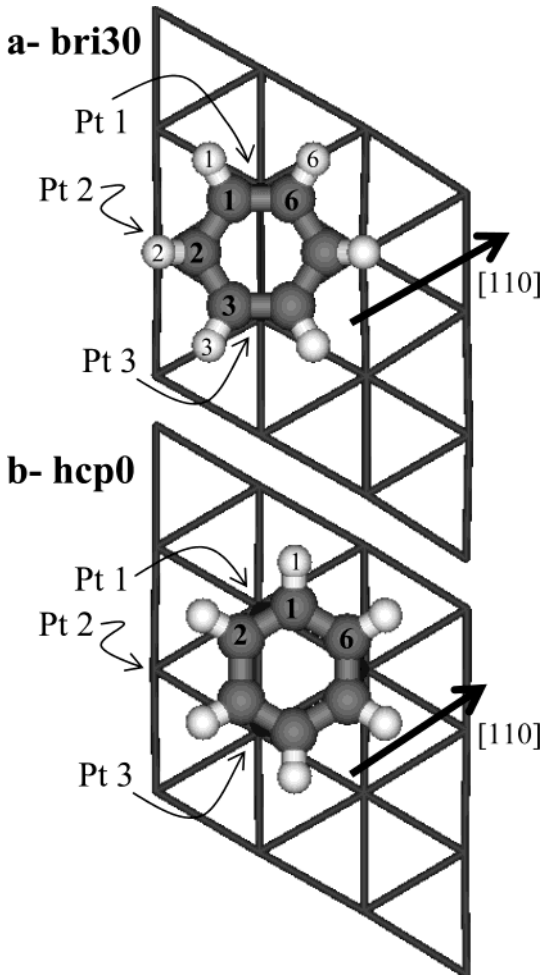

Figure 1. The two most stable adsorption configurations of benzene on the (111) surfaces of Pt, Pd, Ni, Rh: (a) bri30 configuration and (b) hcp0 configurations.

TABLE 1: Adsorption Energy of Benzene in a bri30 Configuration[a] on Pt(111), Pd(111), Rh(111), and Ni(111)[b], and Its Decomposition into Distortion Energy of the Molecule, Distortion Energy of the Surface, and Interaction Energy between the Distorted Molecule and the Distorted Surface

	Pt(111)	Pd(111)	Rh(111)	Ni(111)[b]
adsorption energy (eV)	−0.90	−1.19	−1.53	−1.00
distortion energy of molecule (eV)	1.51	0.89	1.26	
d C_1-C_2 gas phase: 1.40 (Å)	1.47	1.45	1.46	1.45
d C_1-C_6 gas phase: 1.40 (Å)	1.43	1.43	1.43	1.44
α $C_1H_1/C_6C_1C_2$ (°)	15	14	16	
α $C_2H_2/C_1C_2C_3$ (°)	37	27	32	
distortion energy of surface (eV)	0.33	0.14	0.29	
d M_1-M_2 clean slab (Å)	2.82	2.80	2.72	2.50
d M_1-M_2 (Å)	2.85	2.81	2.74	
d M_1-M_3 (Å)	3.04	2.97	2.89	
dd 1st layer−2nd layer (Å)	+0.028	−0.005	+0.052	
dd 2nd layer−3rd layer (Å)	+0.027	+0.005	−0.006	
metal−molecule interaction energy (eV)	−2.74	−2.23	−3.08	
d C_1-M_1 (Å)	2.22	2.23	2.20	2.05
d C_2-M_2 (Å)	2.18	2.20	2.19	

[a] See Figure 1 for atom numbering. [b] From ref 30. Different geometric characteristics are given: d - distance; α- out-of-plane angle; dd - average variation of the interlayer distances relative to the clean relaxed surface.

TABLE 2: Adsorption Energy of Benzene in a hcp0 Configuration[a] on Pt(111), Pd(111), Rh(111), and Ni(111)[b], and Its Decomposition into Distortion Energy of the Molecule, Distortion Energy of the Surface, and Interaction Energy between the Distorted Molecule and the Distorted Surface

	Pt(111)	Pd(111)	Rh(111)	Ni(111)[a]
adsorption energy (eV)	−0.67	−1.03	−1.51	−0.94
distortion energy of molecule (eV)	0.87	0.61	0.86	
d C_1-C_2 gas phase: 1.40 (Å)	1.43	1.43	1.43	1.43
d C_1-C_6 gas phase: 1.40 (Å)	1.46	1.45	1.46	1.45
α $C_1H_1/C_6C_1C_2$ (°)	19	16	19	
distortion energy of surface (eV)	0.35	0.13	0.37	
d M_1-M_2 clean slab (Å)	2.82	2.80	2.72	2.50
d M_1-M_3 (Å)	2.92	2.88	2.78	
d M_1-M_2 (Å)	2.87	2.83	2.76	
dd 1st layer−2nd layer (Å)	+0.016	−0.013	+0.034	
dd 2nd layer−3rd layer (Å)	+0.023	+0.005	+0.009	
metal−molecule interaction energy (eV)	−1.90	−1.76	−2.74	
d C_1-M_1 (Å)	2.22	2.24	2.20	2.07
d C_2-M_2 (Å)	3.16	3.09	3.07	

[a] See Figure 1 for atom numbering. [b] From ref 30. Different geometric characteristics are given: d - distance; α - out-of-plane angle; dd - average variation of the interlayer distances relative to the clean relaxed surface.

TABLE 3: Computed Frequencies and Intensities for the A_1 Vibrational Modes in the Case of the bri30 Adsorption Configuration of Benzene on Pt(111), Pd(111), and Rh(111)

		Pt(111)		Pd(111)		Rh(111)	
mode[a]	description[b]	ν (cm^{-1})	intensity[c]	ν (cm^{-1})	intensity[c]	ν (cm^{-1})	intensity[c]
ν_1	CH str.	3103	37	3113	36	3093	39
ν_2	ring str.	826[e]	159	881[e]	2	870	0.3
ν_4	aop bend.	803	132	716	161	754	70
ν_{15}	CH str.	3042	7	3060	3	3035	12
ν_{16}	CH bend;	1430	5	1445	8	1432	13
ν_{17}	ring deform.	1134	1	1130	0.1	1124	0.5
ν_{18}	ring deform.	566	4	551	2	546	7
ν_{19}	aop bend.	891[e]	42	825[e]	118	829	176
ν_{20}	aop bend.	501	0.1	455	∼0	479	5
ν_{C-M}		358[d]		322[d]		374[d]	
		352[d]		309[d]		367[d]	
		327	19	289	2	351	63

[a] Numbering of modes from ref 53. [b] Str.: stretching; bend.: bending; aop: out-of-plane; deform.: deformation. [c] Arbitrary units. [d] Non A_1 molecule-surface modes. [e] Mixed modes with uncertain attribution.

LEED analysis. Nevertheless, the bri30 structure is in excellent agreement with the STM images,[11−13] which also point out the hcp0 case as a metastable solution. Other theoretical studies, in extended Hückel theory[14,28] or DFT on a platinum cluster[1] show also a preference for the bri30 adsorption structure.

III.2. Benzene on Pd(111). In the case of the Pd(111) surface, the energy difference between the most stable (E_{ads}(bri30) = −1.19 eV) structure and the second one (E_{ads}(hcp0) = −1.03 eV) is reduced compared to Pt(111). This suggests that, as in the case of the adsorption on palladium, the benzene molecules can be adsorbed for a large fraction on a bri30 position, and for another part on a hcp0 position. Benzene adsorption on Pd-(111) has been studied from TDS;[25] whatever the coverage, the TDS shows two different benzene peaks. The authors conclude that the two peaks may be due either to a rapid redistribution or to repulsive adsorbate interaction. One alternative explanation could be the coadsorption of bri30 and hcp0 benzene conformations, which could occur, considering the low energy differences between these two most stable structures. Recent studies for

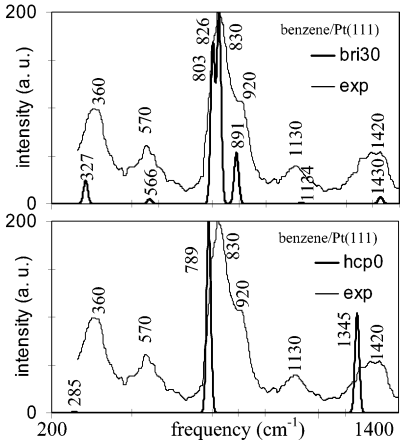

Figure 2. Calculated vibrational spectra for benzene chemisorbed on a Pt(111) surface for the two most stable adsorption structures, bri30 and hcp0 (see Figure 1), with a Gaussian broadening of 18 cm^{-1}. These spectra are compared to the experimental HREELS spectrum reproduced from ref 7.

TABLE 4: Computed Frequencies and Intensities for the A_1 Vibrational Modes in the Case of the hcp0 Adsorption Configuration of Benzene on Pt(111), Pd(111), and Rh(111)

		Pt(111)		Pd(111)		Rh(111)	
mode[a]	description[b]	ν (cm^{-1})	intensity[c]	ν (cm^{-1})	intensity[c]	ν (cm^{-1})	intensity[c]
ν_1	CH str.	3125	48	3120	47	3113	61
ν_2	ring str.	860	0	881	54	870	5
ν_4	aop bend.	789	257	727	288	762	185
ν_9	ring str.+ CH bend.	1345	133	1339	47	1339	36
ν_{10}	ring str.	1154	0.3	1142	0.4	1141	0.4
ν_{C-M}		309[d]		282[d]		366[d]	
		306[d]		279[d]		362[d]	
		285	1	263	5	344	99

[a] Numbering of modes from ref 53. [b] Str.: stretching; bend.: bending; aop: out-of-plane; deform.: deformation. [c] Arbitrary units. [d] Non A_1 molecule-surface modes.

CO adsorption on Pt(111) have shown that GGA-DFT can yield an error of 0.1−0.2 eV for the comparison of adsorption between sites,[40] a value comparable to the difference found here. Hence, the calculation of vibrational frequencies is of great importance to confirm the site preference obtained from total energy calculations. The relative energy of the bridge and hollow sites could also depend on the molecular coverage on the surface, as previously suggested on Pt(111)[1].

The experimental HREELS spectra from Waddill et al.[25,41] show seven peaks, at 265, 470, 720, 810, 1100, 1410, and 2990 cm^{-1}. Table 3, Table 4 and Figure 3 present our computed results for the vibrations and the simulated spectra in the bri30 and hcp0 configurations. We can first confirm that the first experimental loss at 265 cm^{-1} can be attributed to a ν_{C-Pd} vibration: our results show vibration frequencies at 289 cm^{-1} in the case of a bri30 adsorption and 263 cm^{-1} in the case of a hcp0 one. All the other experimental peaks can be better correlated with computed vibration modes of the bri30 structure. The experimental spectra show two peaks with high intensities at 720 and 810 cm^{-1}. These can be related with the computed vibration modes at 716 and 825 cm^{-1} obtained for a bri30 adsorption structure, with high intensities. The first energy loss can be assigned to the out-of-plane bending ν_4 mode (in the nomenclature from ref 42), while the second one can be associated with a mixed mode between the ν_2 (ring stretching) and the ν_{19} (out-of-plane bending) modes. This surprising mixing

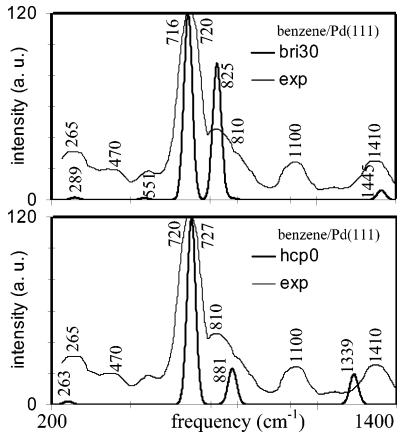

Figure 3. Calculated vibrational spectra for benzene chemisorbed on a Pd(111) surface for the two most stable adsorption structures, bri30 and hcp0 (see Figure 1), with a Gaussian broadening of 18 cm^{-1}. These spectra are compared to the experimental HREELS spectrum reproduced from ref 25.

is permitted because the two modes have the same A_1 symmetry in the adsorption geometry. The high intensity of these two modes can be explained by the out-of-plane displacement of the hydrogen atoms, which involves an important variation of the dipolar moment projected on the direction perpendicular to the surface. The intensity of the other peaks is lower, as in the computed modes. The relatively large loss at 3000 cm^{-1} is found to be a superposition of two modes, the C−H stretching modes ν_1 at 3113 cm^{-1} and ν_{15} at 3060 cm^{-1}. In this case, the difference between the experimental and the computed frequencies can be attributed to the anharmonicity factor that we did not take into account, and that could usually play a significant role for the hard C−H stretching modes. The experimental peaks at 1410, 1100 and 470 cm^{-1} can be correlated respectively to the ν_{16} (C−H bending), ν_{17} (deformation of the ring) and ν_{20} (out-of-plane bending) modes, computed at 1445, 1130, and 455 cm^{-1}, respectively, although the simulated intensity is very small for the two last peaks. Finally, as in the case of the adsorption of benzene on Pt(111), the bri30 adsorption structure can explain the HREELS spectrum, in agreement with the total energy results. Nevertheless, the spectrum shows a nonlisted shoulder at ∼900 cm^{-1}. This shoulder suggests that a fraction of the benzene molecules is adsorbed in a hcp0 structure: this shoulder can be explained by the computed ν_2 mode at 881 cm^{-1} for the hcp0 configuration. In this case, the experimental spectra should also show a peak in the surroundings of the previously calculated ones for bri30 at 727 and 1339 cm^{-1}. The first peak is included in the dominant experimental one at 720 cm^{-1}, while the second one may be in the noise just below the experimental peak at 1410 cm^{-1}. Hence, the best interpretation of the experimental HREELS spectrum indicates a predominant bri30 adsorption configuration, with a small fraction of hcp0 molecules, and the largest peak at 720 cm^{-1} cannot help us to determine unequivocally the preferred adsorption structure. It is clear that an improved resolution, which can now be achieved with modern experiment, could help to separate the various features.

Several LEED experiments have been performed on the Pd(111)−(3 × 3)-C_6H_6+2CO coadsorption structures.[43,23] None has been done for the adsorption of pure benzene on Pd(111). In each case, a hollow position, with an azimuthal angle of 0° (hcp0) is found to give the best *R*-factors, with little[43] or no Kekulé[23] distortion. As we saw, the two most stable positions are the bri30 and hcp0 ones, but with a small difference. We can argue that in the presence of CO, the adsorption in the hollow position becomes more stable than the other one. The geometric characteristics are in good agreement with ours for the hcp0 adsorption structure. The C−C bond above the Pd atom is computed to be $d_{C-C} \sim 1.43$ Å, while the LEED data give a 1.40 ± 0.10 Å[43] or 1.40 ± 0.15 Å,[23] and the C−C bonds bridging two palladium atoms is found to be $d_{C-C} \sim 1.46$ Å, and 1.46 ± 0.10 Å[43] and 1.40 ± 0.15 Å[23] for the LEED studies. However, the difference is slightly larger for the Pd−C distance, with a calculated value of 2.20 Å and a LEED value of 2.39 ± 0.05 Å.[43,23]

A recent paper[44] about the scanning tunneling microscopy (STM) images of benzene molecules adsorbed on Pd(111) in a $c(2\sqrt{3} \times 3)$−*rect*-C_6H_6 structure at electrode surfaces shows a benzene molecule in a pseudo-triangular shape and slightly tilted. At lower coverage, in a (3 × 3)−C_6H_6 structure, the molecule is identified as a set of three spots, each spot above a palladium atom. This study seems to favor the hcp conformation, but this can be explained as follows: (i) in the first case, by the high coverage, and (ii) by the coadsorption with water molecules, that are seen as extra spots in images.

After comparison with the adsorption of a benzene molecule on Pt(111), in which case the adsorption in the bri30 site leaves no doubt, the case of Pd(111) is more open, in particular for the coadsorption of benzene with CO or with H_2O, which seems to favor the hollow site. This is well in line with the smaller difference in adsorption energy between these two structures.

III.3. Benzene on Rh(111). When adsorbed on Rh(111), the benzene molecule can achieve both hcp0 and bri30 structures with almost the same computed adsorption energy: E_{ads}(bri30) = −1.53 eV and E_{ads}(hcp0) = −1.51 eV. As in the case of the adsorption on Pd(111), the benzene molecule will adsorb for a part in a hcp0 position and for the other in a bri30 one. Minot et al., through Extended Hückel calculations on Rh clusters, showed that the hcp0 configuration is the best one on a Rh_6 cluster, with a binding energy of 0.99 eV. Nevertheless, no full optimization of the bri30 configuration has been done, which forbids any comparison. In the hcp0 case, a Kekulé distortion is found, with C−C distances of 1.50 and 1.64 Å and C−Rh distances of 2.06 Å, while our study gives a more reasonable length of 1.43 and 1.48 Å for the C−C bonds and 2.20 Å for the C−Rh bonds. In the bri30 adsorption case, the out-of-plane CH−CCC angle is found to be 20°, while our study shows a 32° value. An optimization of the geometry of this structure, in particular of the out-of-plane angle, may lead to a more stable configuration.

Table 3 and Table 4 display the computed vibrational frequencies for benzene adsorbed on Rh(111) in the bri30 and hcp0 conformations, respectively. Figure 4 shows the comparison of the computed and experimental HREELS[45,16] spectra. The experimental spectra present 7 peaks at ∼3000, 1430, 1330, 1115, ∼805, 545, and 345 cm^{-1} [16] and a shoulder at 880 cm^{-1}.[45] Under high resolution, the peak at ∼805 cm^{-1} is decomposed into two separated peaks at 776 and 819 cm^{-1} [45] or at 775 and 805 cm^{-1}.[16] As in the case of the adsorption on Pt(111) and Pd(111) surfaces, the losses at ∼3000 cm^{-1} are not well described in our calculation, since we do not consider the anharmonicity factor. The major experimental loss, attributed to the ν_4 mode, at ∼810 cm^{-1}, separated into two peaks at 776 and 819 cm^{-1} (or 775 and 805 cm^{-1}), could be explained by the bri30 adsorption case, for which the calculation gives two losses, attributed to the out-of-plane ν_4 and ν_{19} modes, with high intensities at 754 and 829 cm^{-1}. Nevertheless, this predominant peak shows a shoulder on the right side, at ∼880 cm^{-1}, listed for the ν_2 mode. This shoulder can be explained

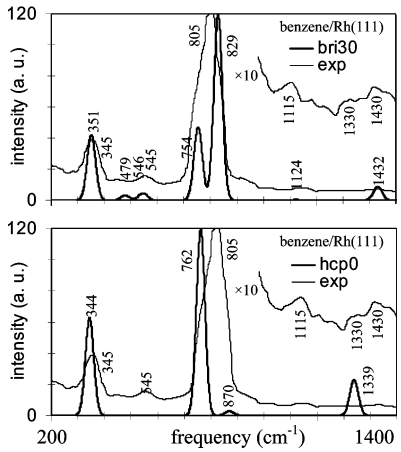

Figure 4. Calculated vibrational spectra for benzene chemisorbed on a Rh(111) surface for the two most stable adsorption structures, bri30 and hcp0 (see Figure 1), with a Gaussian broadening of 18 cm^{-1}. These spectra are compared to the experimental HREELS spectrum reproduced from ref 16.

by the presence of a benzene molecule in the hcp0 configuration, as in the case of the adsorption on Pd(111). In this hcp0 configuration, two peaks are computed, at 762 and 870 cm^{-1}, for the ν_4 (out-of-plane bending) and ν_2 (ring stretching) modes. They may be seen in the experimental shoulders, respectively, at 776 cm^{-1} (together with the peak at 754 cm^{-1} from the bri30 structure) and at 880 cm^{-1}. This agrees with the proposition of Mate et al.;[16] the mode at 805 cm^{-1} is assigned to the CH bending mode of benzene in a bridge site, while the 775 cm^{-1} frequency is assigned to a small proportion of benzene adsorbed at 3-fold hollow sites. The second largest experimental loss, at 345 cm^{-1} for the metal−carbon elongation mode, can be correlated simultaneously with the computed peaks at 351 cm^{-1} for the bri30 adsorption case, and at 344 cm^{-1} for hcp0, both describing the metal−carbon elongation modes. The experimental peaks at 545, 1115, and 1430 cm^{-1}, attributed by the authors to the ν_{C-Rh}, ν_{10}, and ν_{13} modes, respectively, correspond to the computed frequencies at 546, 1124, and 1432 cm^{-1} for the bri30 adsorption geometry. The mode attribution of the peaks is different from ours, as we attribute them to the molecular ν_{18} (ring deformation), ν_{17} (ring deformation), and ν_{16} (CH bending) modes. Moreover, the loss at 1330 cm^{-1} can only be explained again by the presence of benzene in the hcp0 configuration, where a loss at 1339 cm^{-1} is found and is attributed to a ring stretching mode.

Finally, the computation of the vibrational frequencies is powerful. It allows us to propose a new attribution of the different losses, and the comparison of the experimental and the computed spectra leads us to conclude that in the experimental conditions, both bri30 and hcp0 benzene structures are present simultaneously on the surface. Moreover, the presence of bri30 and hcp0 structures is in agreement with their equivalent adsorption energies. Going from the adsorption on Pt(111), to Pd(111) and Rh(111), the proportion of hcp0 structures deduced from the HREELS spectra increases, in agreement again with the variation of the difference of adsorption energies on these three surfaces.

Scanning tunneling microscopy images of benzene on Rh(111)[46] show that benzene does not form a well-ordered overlayer, even at saturation coverage, and that the molecules appear as ring-like structures. However, some molecules cannot be seen, which is apparently due to a faster diffusion than the scanning rate. Nevertheless, the ring-like structures observed in small ordered domains cannot be explicitly attributed to one or another adsorption structure. A theoretical simulation of STM images of bridged molecules would be helpful in this respect.

In a LEED study of pure benzene adsorption, a $(2\sqrt{3} \times 3)$-*rect* structure is observed,[45] and a bri30 conformation is proposed,[16] but no geometry optimization has been done.

Finally, from the computation of HREELS, LEED, and DFT calculations, it can be concluded that when adsorbed on Rh(111), pure benzene adopts a bri30 configuration in a $(2\sqrt{3} \times 3)$*rect* structure in small domains, with a fast reorganization, and a hcp0 configuration in disordered domains.

III.4. Coadsorption of Benzene and CO on Rh(111). In the case of coadsorption of benzene and CO on Rh(111), just one high peak at 780 or 805 cm^{-1} is observed in HREELS,[16] depending on the layer structure, which shows that the coadsorption implies that the benzene adsorbs in one configuration only, rather than in a mixture of bri30 and hcp0 adsorption structures.

Moreover, still in the case of coadsorption with carbon monoxide, STM studies show that the mobility of benzene decreases, and ordered domains with both $c(2\sqrt{3} \times 4)$*rect* or (3×3) structure are observed, depending on the amount of preadsorbed CO.[46,21] In the case of a preadsorption of benzene and then an adsorption of CO, the $c(2\sqrt{3} \times 4)$*rect* structure is observed, with one CO molecule per unit cell, while the benzene adsorption on CO-precovered surfaces leads to a (3×3) overlayer structure, with two CO molecules per unit cell. In these two last cases, a hcp0 adsorption configuration is proposed by experiments[21] and theoretical simulations from Sautet and Joachim,[22] since the benzene molecules appear as three-bump schemes.

LEED experiments also detail the possibility for a benzene molecule to coadsorb with CO either in $c(2\sqrt{3} \times 4)$*rect* or (3×3) structures.[47−50] In both cases, benzene is found to adsorb in a hcp0 configuration, with a strong Kekulé distortion. Hence, in the $c(2\sqrt{3} \times 4)$*rect* structure, the best *R*-factor is obtained for a C−C bond length of 1.33 ± 0.15 Å (for bonds on top of a rhodium atom) and 1.81 ± 0.15 Å (for bonds between rhodium atoms), and a Rh−C bond length of 2.35 ± 0.15 Å.[49] In the (3×3) structures, the optimization of the geometry from LEED leads again to a hcp0 structure with on-top and bridging C−C bond lengths of 1.46 ± 0.15 and 1.58 ± 0.15 Å, respectively, and Rh−C bond lengths of 2.30 ± 0.15 Å.[50] These structures are optimized in the presence of CO molecules. We can nevertheless compare them to those we found for hcp0 benzene. In our computational optimization, we found on-top and bridging C−C bond lengths of 1.43 and 1.46 Å, respectively, while the Rh−C bond length is found to be 2.20 Å. The very good agreement of the vibrational spectra presented previously and the large error bar in LEED allows us to consider our lengths as correct. As a result, the Kekulé distortion from DFT is not as large as in the LEED conclusions.

To have an idea about the role of the CO−benzene coadsorption on the Rh(111) surface, calculations of the coadsorption simulations have been performed. We choose a (3×3) cell, as represented in Figure 5. In the case of hcp0 adsorption of benzene molecules, two CO molecules are put on hollow hcp sites (see Figure 5b), as suggested by LEED conclusions from ref 16 which implies a coverage of 1/9 ML in benzene and 2/9 ML in CO. In the case of bri30 adsorption of benzene, we choose for computation the same (3×3) cell, with one benzene and two CO in bridge position (Figure 5a). The results for adsorption energies are summarized in Table 5. The adsorption of CO on Rh is more favorable on a hollow hcp site ($E_{ads} \sim -1.98$ eV for one CO) than on a bridge one ($E_{ads} \sim -1.87$ eV

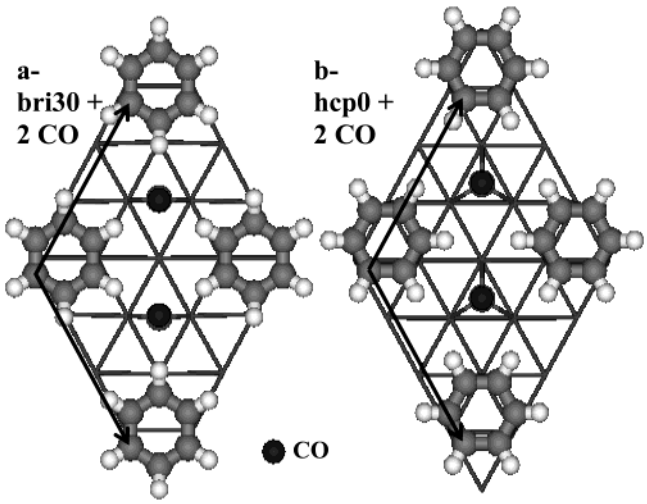

Figure 5. Benzene and carbon monoxide (CO) coadsorption on cell: (3×3)-C_6H_6+2CO on Rh(111). (a) benzene molecules in bri30 configuration and CO in bridge sites. (b) Benzene molecules in hcp0 configuration and CO in hollow sites. The arrows represent the lattice vectors.

TABLE 5: Decomposition of the Coadsorption Energy (eV) of Benzene and Carbon Monoxide on Rh(111), in (3×3)-C_6H_6+2CO Cell

	C_6H_6+2CO on Rh(111) (3×3)[c]	C_6H_6 on Rh(111) (3×3)[d]	*2*CO on Rh(111) (3×3)+C_6H_6[e]	*2*CO on Rh(111) (3×3)[f]	C_6H_6 onRh(111) (3×3)+2CO[g]
bri30[a]	−5.12	−1.53	−3.59	−3.73	−1.39
hcp0[b]	−5.58	−1.51	−4.07	−3.96	−1.62

[a] Benzene molecules in bri30 conformation and CO in bridge sites (see Figure 5a). [b] Benzene molecules in hcp0 and CO in hollow sites (see Figure 5b). [c] Energy (eV) of coadsorption of one benzene and two CO on naked Rh(111) slab. [d] Adsorption energy (eV) of one benzene on naked Rh(111). [e] Adsorption energy (eV) of two CO on benzene recovered Rh(111). [f] Adsorption energy (eV) of two CO on naked Rh(111). [g] Adsorption energy (eV) of one benzene on CO recovered Rh(111).

for one CO). These values are in very good agreement with those found in DFT by Mavrikakis et al.,[51] who found E_{ads}(hollow hcp) = −1.99 eV and E_{ads}(bridge) = −1.89 eV. This study showed also that the top adsorption site is the most stable (E_{ads}(top) = −2.04 eV). Note, however, that the difference with the bridge site is small. The adsorption of benzene on CO-preadsorbed Rh(111) is easier on hcp0 (E_{ads} = −1.62 eV) than on bri30 (E_{ads} = −1.39 eV). The energy difference (0.23 eV) appears large, compared to the pure benzene on Rh(111) adsorption (0.02 in favor of bri30). It compares well, however, with the cost to move two CO molecules from a hollow site to a bridge site (0.22 eV). Moreover, the adsorption energies of CO on benzene-preadsorbed Rh(111) are larger for the hollow hcp site (−0.06 eV) and lower for the bridge site (+0.07 eV). Hence, there are cooperative effects in the adsorption of CO and benzene on Rh(111), and finally, the coadsorption of two CO and one benzene is more favorable in the case of hcp structure (E_{ads} = −5.58 eV) as compared to the case of bridge structure (E_{ads} = −5.12 eV). This can explain that for coadsorbed CO and benzene molecules, the benzene is experimentally seen in a hcp0 structure. To explain the different experimental observation, the same trend is supposed to occur in the case of benzene and CO or H_2O coadsorption on Pd(111), but not on Pt(111).

IV. Discussion and Trends

It is clear from the previous section that the energy differences between the various adsorption sites of benzene depend on the metal. Insights into the differences can be obtained through a decomposition of the energies, and an analysis of the metal−substrate vibrational modes. The detailed electronic structures can also help us to understand these variations, in terms of interactions between the metal *d*-band and the molecule π orbitals.

IV.1. Energetic, Geometric, and Vibrational Analysis. We have previously shown[29] that a decomposition of the energy can be helpful to understand the adsorption energy. This decomposition is done in three parts: $E_{ads} = E_{dist}$(molecule) + E_{dist}(surface) + $E_{interaction}$. E_{dist}(molecule) is the distortion energy of the molecule, calculated as the difference between the energy of the molecule in the gas-phase geometry and the energy of the molecule still isolated and distorted as in the adsorption geometry. E_{dist}(surface) is the distortion energy of the surface, computed as the difference between the energy of the clean relaxed surface and the energy of the isolated surface in the distorted geometry from molecular adsorption. The last part of the adsorption energy, $E_{interaction}$, is the interaction energy between the molecule and the surface, calculated as the difference between the adsorption energy and the sum of both distortion energies of molecule and surface. This decomposition is reported in Table 1 and Table 2 for the bri30 and hcp0, respectively, for the Pt(111), Pd(111), and Rh(111) surfaces, together with the geometric data.

In both bri30 and hcp0 adsorption cases, the distortion energy of the surface is lower for the adsorption on Pd(111) (E_{dist}(surface) = 0.14 and 0.13 eV, respectively), than on Pt(111) (0.33 and 0.35 eV, respectively) and Rh(111) (0.29 and 0.37 eV, respectively). This distortion energy is correlated to the average variation of the distance between the metal layers in the case of the clean surface and of the adsorbate−substrate complex. The adsorption on Pd(111) is the only one that implies a decrease of the distance between the first and the second layers (−0.005 and −0.013 Å for bri30 and hcp0 adsorption structures, respectively), while in the case of the Pt(111) and Rh(111) surfaces, this value is positive and larger (+0.028 Å for bri30 and +0.016 Å for hcp0 for Pt(111) and +0.052 Å for bri30 and +0.034 Å for hcp0 for Rh(111)). The distance between the second and the third layers varies also less in the case of the adsorption on Pd(111) than in the case of Pt(111) and Rh(111). We can suggest that a larger and positive variation of the distance in the cases of Pt and Rh implies a worse interaction between the d electrons of the metal atoms of the different layers, and then a larger distortion energy.

The distortion energy of the benzene molecule is also smaller in the case of its adsorption on Pd(111) than on Pt(111) or on Rh(111). For the bri30 adsorption structure, it is E_{dist}(molecule) = 0.89 eV on Pd(111), 1.51 eV on Pt(111), and 1.26 eV on Rh(111). The adsorption geometries show different C−C bond lengths, with an average of 1.43 Å on Pd, 1.46 Å on Pt, and 1.45 Å on Rh, while the relaxed gas-phase structure shows a C−C bond length of 1.40 Å. They also show different out-of-plane CH/CCC angles, with a mean value of 18° for Pd, 22° for Pt, and 21° for Rh. The distortion energy is then clearly correlated to the geometry characteristics: the longer are the C−C bonds and larger the out-of-plane CH/CCC angles, the larger is the distortion energy of the molecule. In the case of the adsorption in the hcp0 configuration, the distortion energies of the molecule are much lower, E_{dist}(molecule) = 0.87 eV on Pt(111), 0.61 eV on Pd(111), and 0.86 eV on Rh(111). This is

also clearly linked to the geometric data. The average C−C bond length and out-of-plane CH/CCC angle are worth, respectively, 1.45 Å and 19° on Pt(111), 1.44 Å and 16° on Pd(111), and 1.45 Å and 19° on Rh(111). The distortions for benzene in the hcp0 conformation on Pt(111) and Rh(111) are similar in the bri30 conformation on Pd(111), the distortion energies being also equivalent (E_{dist}(molecule) ∼ 0.88 eV). The distortion in the case of the adsorption on Pd(111) in the hcp0 conformation is less marked, which implies a lower distortion energy.

In addition, we can notice that the distortion energies of the surface are similar for the bri30 and the hcp0 adsorption structures, but the distortion energies of the molecule are much smaller in the case of the adsorption in the hcp0 site than on the bri30 site.

The interaction energies between the metal surface and the molecule are larger for the adsorption on bri30 sites than on hcp0 sites. The interaction energies are mainly due to the interaction between the π electrons of the aromatic molecule and the *d*-band of the metal. This will be discussed below, in the electronic analysis section. As already shown for the different adsorption possibilities of benzene on Pt(111)[29] and of thiophene on Ni(110),[52] the interaction energies are related to the number of short molecule−metal bonds. This has no influence in our study, since, as detailed in the geometric Table 1 and Table 2, in both adsorption configurations bri30 and hcp0, the number of short bonds is the same (6) and their lengths are similar (with an average of 2.21 Å and 2.22 Å for bri30 and hcp0, respectively, on Pt(111), 2.22 and 2.24 Å on Pd(111), and 2.20 and 2.20 Å on Rh(111)). Nevertheless, in the case of the adsorption on bri30 sites, four different metal atoms are involved in bonds, while only three are involved in the case of the hcp0 structure. This can lead to larger interaction energies in the case of the bri30 conformations than in hcp0 ones. Moreover, the interaction energies divided by the number of metal atoms involved in bonds are $E_{interaction}/N_{metal} = -0.69$, -0.56, and -0.77 eV for the adsorption on the bri30 site on Pt(111), Pd(111), and Rh(111), respectively, and $E_{interaction}/N_{metal} = -0.63$, -0.59, and -0.91 eV for the adsorption on the hcp0 site on Pt(111), Pd(111), and Rh(111), respectively. This shows that for the adsorption on Pt(111), the interaction energy by platinum atom in the case of the bri30 conformation is larger than in the case of hcp0. On the contrary, on Pd(111), the interaction energy by palladium atom is slightly larger for the hcp0 configuration than for bri30 one. And for Rh(111), it is really larger for hcp0 than for bri30. This clearly illustrates the trend for the adsorption site from a platinum surface clearly favoring the bridge site to a rhodium surface where bridge and hollow sites are equivalent.

The comparison of the adsorbate−substrate vibrational frequencies is also interesting in the analysis of those interaction energies. In the case of the adsorption on the bri30 position (Table 3), the average of the three adsorbate−substrate frequencies is 346 cm^{-1} on Pt(111), 307 cm^{-1} on Pd(111), and 364 cm^{-1} on Rh(111). On hcp0 positions (Table 4), it is 300 cm^{-1} on Pt(111), 275 cm^{-1} on Pd(111), and 357 cm^{-1} on Rh(111). Classically, the stronger the bond, the larger is the associated vibrational frequency. In our case, for the bri30 adsorption configuration, the interaction energy between the benzene molecule and the surface is larger for the adsorption on Rh(111) than on Pt(111), and than on Pd(111). The average frequencies follow the same order. The same analysis can be done for the hcp0 adsorption case. Moreover, for each metal, the frequencies are larger for the bri30 adsorption case than for the hcp0 one, as the interaction energies are larger for the bri30 adsorption case than for the hcp0 one. Hence, on Pt(111) the difference between the average vibrational frequency in bri30 and hcp0 configurations is worth 46 cm^{-1}, 32 cm^{-1} on Pd(111), and 7 cm^{-1} on Rh(111). The same order is found for the difference between the interaction energies for the bri30 and hcp0 configurations (0.84, 0.47, and 0.34 eV, respectively), and for the difference between the interaction energies by metal atom with an adsorption on the bri30 and hcp0 sites (0.05, 0.03, and -0.14 eV, respectively).

An important outcome of these energetic studies is that there is no direct relation between the interaction energy and the final adsorption energy. A strong interaction energy is indeed associated with a large deformation energy for the molecule. However, as the adsorption energy is a compromise between the destabilizing deformations and the stabilizing interaction, a strong interaction does not mean necessarily a strong adsorption. For example, the adsorption energy is larger on Pd than on Pt, while the distortion energy and interaction energy are both smaller (see Table 1 and Table 2). We can then classify the different structures and metal surfaces according to their interaction energy. The bridge adsorption of benzene leads predominantly to a strong interaction, while the 3-fold configuration leads to a weaker one: the distortion energies of the benzene molecule are at least 0.4 eV and the interaction energies are at least -0.3 eV larger in the case of bridge adsorption. On the other hand, the rhodium and platinum surfaces lead to a strong interaction and the palladium surface to a weaker one. The next section will detail these differences in terms of electronic interactions.

IV.2. Electronic Analysis. *a. Density of States*. The projected density of states (PDOS) on the atomic orbitals of the carbon and the metal atoms are shown in the Figure 6, Figure 7, and Figure 8, with the energy scale relative to vacuum level. The bri-30 and the hcp-0 structures are considered on the Pt, Pd, and Rh surfaces.

In each figure, the first window (a-1 or b-1) represents the PDOS on the $2p_z$ atomic orbitals of the carbons of the isolated benzene molecule (dashed lines), or distorted as in the bri30 adsorption configuration (continuous lines in a-1) or in the hcp0 adsorption configuration (continuous lines in b-1). The molecular distortion on the surface results in a symmetry lowering and in a marked reduction of the gap between the highest occupied molecular orbitals (HOMO) and the lowest unoccupied ones (LUMO), as previously shown in the case of benzene adsorption on Pt(111).[1] These HOMO and LUMO orbitals are doubly degenerate in the gas phase, the degeneracy being lifted in the bri30 distortion, but not in the hcp0. As the distortion is increased, the aromatic character is lowered and the energy difference between the HOMO and the LUMO decreases. For the bri30 conformation, the HOMO−LUMO gaps for the distorted molecules are 3.94 eV on Pt(111), 4.38 eV on Pd(111), and 4.16 eV on Rh(111), which is linked to the distortion energies, 1.51, 0.89, and 1.16 eV, respectively. For the hcp0 conformation on Pt(111), Pd(111), and Rh(111), the energy gaps are 4.50, 4.62, and 4.50 eV, respectively, for distortion energies of 0.87, 0.61, and 0.86 eV, respectively. Concomitantly, the mixing between the $2p_z$ orbitals of carbon atoms and the other atomic orbitals increases with the distortion. This appears in the PDOS as small contributions of $2p_z$ on orbitals of pure s character in the gas phase. For the strongly distorted cases (bri30 on Pt(111) and bri30 on Rh(111)), such contributions become large, while they are modest for the less distorted structure, such as hcp0 on Pd(111).

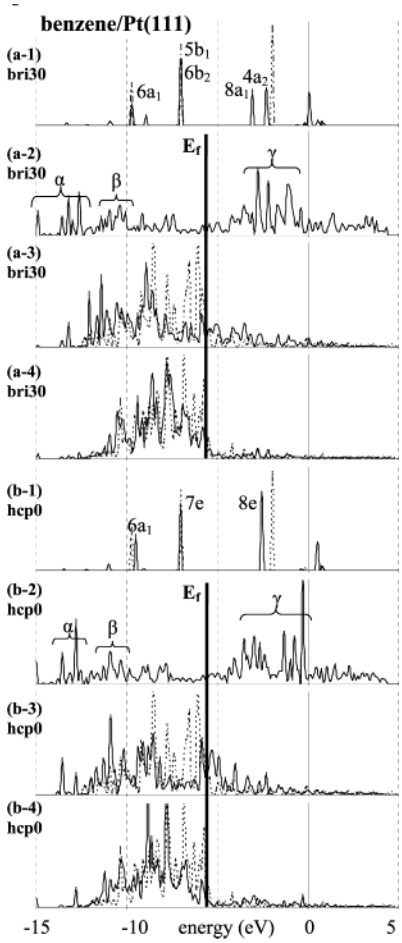

Figure 6. Density of states (PDOS) projected on the atomic orbitals of benzene and Pt(111) surface in (a) bri30 and (b) hcp0 adsorption configurations. (a-1) and (b-1): PDOS on $2p_z$(C) of benzene in gas phase (dashed line) and in isolated benzene distorted as in the adsorption structure (continuous line) with numbering of molecular orbitals. (a-2) and (b-2): PDOS on $2p_z$(C) of adsorbed benzene. (a-3) and (b-3): PDOS on $6d_{z^2}$(Pt) of the first layer of the bare surface (dashed line) and with adsorbed benzene (continuoud line). (a-4) and (b-4): PDOS on $6d_{xz}+6d_{yz}$(Pt) of the first layer of the clean surface (dashed line) and with adsorbed benzene (continuous line). The zero energy refers to vacuum energy. E_f corresponds to Fermi level.

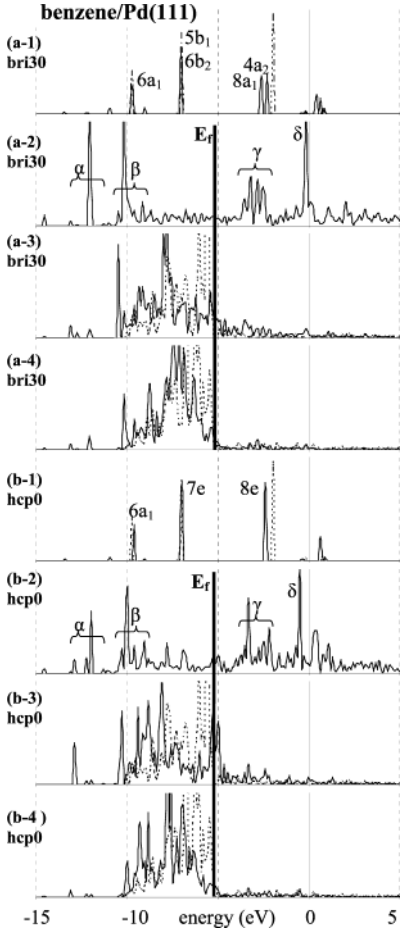

Figure 7. Density of states (PDOS) projected on the atomic orbitals of benzene and Pd(111) surface in (a) bri30 and (b) hcp0 adsorption configurations. (a-1) and (b-1): PDOS on $2p_z$(C) of benzene in gas phase (dashed line) and in isolated benzene distorted as in the adsorption structure (continuous line) with numbering of molecular orbitals. (a-2) and (b-2): PDOS on $2p_z$(C) of adsorbed benzene. (a-3) and (b-3): PDOS on $5d_{z^2}$(Pd) of the first layer of the bare surface (dashed line) and with adsorbed benzene (continuous line). (a-4) and (b-4): PDOS on $5d_{xz}+5d_{yz}$(Pd) of the first layer of the clean surface (dashed line) and with adsorbed benzene (continuous line). The zero energy refers to vacuum energy. E_f corresponds to Fermi level.

The PDOS on the d_{z^2} and the $(d_{xz} + d_{yz})$ orbitals, for the bare surface, are shown as a dashed line on the windows (a-3) and (a-4) and similarly on (b-3) and (b-4), respectively. The energy position of the Fermi level, −5.76, −5.37, and −5.19 eV on Pt, Pd, and Rh, respectively, corresponds to the filling of the energy band. Since Pt and Pd have 10 valence electrons per atom, their *d*-band is nearly full, whereas the *d*-band of Rh, with 9 valence electrons per atom, has more vacant contributions than Pt or Pd. The *d*-bandwidth shows an important difference. The *d*-band of the clean Pd(111) surface is rather narrow (∼5 eV) and shows an energy average of −6.36 eV, estimated by taking into account all the d atomic orbitals. The *d*-band of Pt-(111) is larger (∼6.5 eV) and the energy average is lowered to −7.22 eV, as expected. This is due to the fact that the 6d orbitals of the platinum atom are more diffuse than the 5d orbitals of the palladium atom. The *d*-band of the Rh(111) is even larger (∼6.7 eV) but with an average value of −6.12 eV. The rhodium is more electropositive, and hence has d states at a higher energy and more diffuse orbitals. This explains the larger band. Moreover, the shift to higher energies of the d states is consistent with the reduced d^9 electron count, for an equivalent value of the Fermi level. A consequence of this different bandwidth and this average position can be seen on the energy of the *d*-band bottom. The Pt *d*-band goes down to −13 eV, while that of Pd finishes at −10 eV. The case of Rh is intermediate with a band bottom at −11 eV. It is, hence, already clear that the energy overlaps between d states and benzene orbitals will show important differences upon the three metals.

The first aspect of the orbital mixing upon chemisorption can be seen on the PDOS on the $2p_z$ orbitals of the carbon atom (windows (a-2) and (b-2)). The molecule−surface interaction results in a marked dilution of this atomic orbital contribution over a large range of energies. Three main zones can be underlined. The first one corresponds to discrete bonding states positioned below the *d*-band, mainly associated with the low-lying 6a1 orbital and with mixing of $2p_z$ with s states. The second part is related to states which are delocalized within the *d*-band. While Pt and Rh show a similar behavior in this *d*-band energy range, Pd is singular: it shows a large peak at the *d*-band bottom (−10 eV) and very small $2p_z$ contributions at other energies within the band. This is related to the narrower shape of the *d*-band for this metal, the bonding states being pushed just below the band bottom and hence acquiring a discrete character. The third part is located above the *d*-band, and is

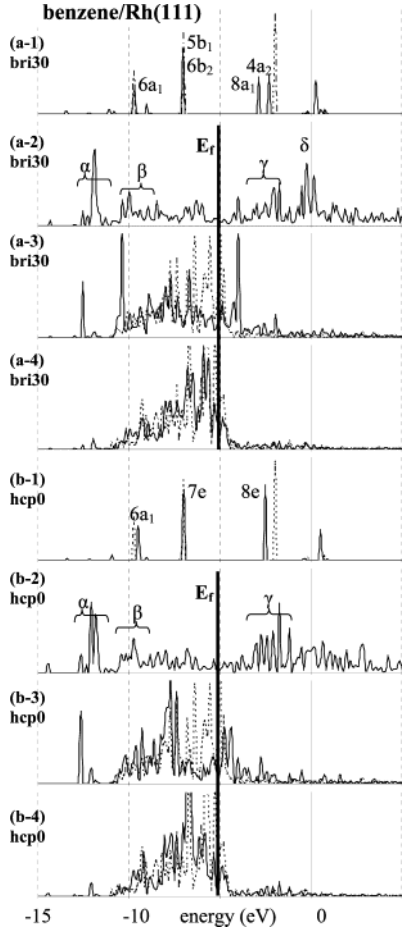

Figure 8. Density of states (PDOS) projected on the atomic orbitals of benzene and Rh(111) surface in (a) bri30 and (b) hcp0 adsorption configurations. (a-1) and (b-1): PDOS on $2p_z$(C) of benzene in gas phase (dashed line) and in isolated benzene distorted as in the adsorption structure (continuous line) with numbering of molecular orbitals. (a-2) and (b-2): PDOS on $2p_z$(C) of adsorbed benzene. (a-3) and (b-3): PDOS on $5d_{z^2}$(Rh) of the first layer of the bare surface (dashed line) and with adsorbed benzene (continuous line). (a-4) and (b-4): PDOS on $5d_{xz}+5d_{yz}$(Rh) of the first layer of the clean surface (dashed line) and with adsorbed benzene (continuous line). The zero energy refers to vacuum energy. E_f corresponds to Fermi level.

associated with vacant contributions, mainly due to the LUMO orbitals, or its mixing with σ orbitals.

A more detailed understanding of the electronic interactions can be gained by considering the projected DOS on the metal atoms which directly interact with benzene. The projections on the d_{z^2} and $(d_{xz} + d_{yz})$ orbitals of such atoms are shown as continuous lines in the windows (a-3), (a-4) and (b-3), (b-4), in comparison with the DOS for the bare surface (dashed lines). The d_{z^2} orbital clearly shows a strong interaction for all three metals: the contribution of states just below the Fermi level is strongly reduced, while additional d_{z^2} DOS is created both at low energy (*d*-band bottom and below) and above the Fermi level. This is mainly the result of the interaction between d_{z^2} and the HOMO of benzene: bonding combinations are shifted to lower energies, while antibonding ones are partially shifted above the Fermi energy. Another reason is the interaction between d_{z^2} and the benzene LUMO, as evidenced by the matching energies between d_{z^2} contributions in (a-3) and LUMO contributions in (a-2). These contributions of d_{z^2} states above the Fermi level decrease in the order Rh > Pt > Pd, well in line with a reduced molecule−surface interaction energy. The $(d_{xz} + d_{yz})$ orbital is less perturbed by the molecule, especially in the cases of Pt and Rh. In the case of Pd, there is a reduction of the DOS for $(d_{xz}+ d_{yz})$ states just below the Fermi level, and increased contribution from mixings at lower energies. However, no clear increase of this band weight is seen above the Fermi level.

Hence, the projected densities of states give important insights in the interactions between the molecule and the surface, and in the effect of a different metal surface.

b. Electron Density. Figure 9 displays the differential electron densities as benzene adsorbs on bri30 and hcp0 configurations on Pt(111). The differential electron density is defined as the difference between the electron distribution of the adsorbate−substrate complex and those of a clean surface and an isolated molecule, both distorted to fit the geometry in the adsorption complex. The first part of the figures displays positive density isosurfaces, i.e., the spatial zones where the electronic population has been increased through adsorption. On the other hand, the second part displays the spatial zones where the charge density decreases when the molecule adsorbs, i.e., the spatial zones depopulated in electrons.

These densities reflect the interactions between surface and molecule, and they can be related with the previous PDOS analysis. Indeed, the population and depopulation of the electronic density come from an interaction between the orbitals of the molecule and those of the slab. As explained before, the occupied π molecular orbitals interact with the d_{z^2}-band of the metallic slab, to form bonding contributions at lower energies and antibonding ones which are, in part, pushed above the Fermi level. As a result these antibonding contributions are vacant, and both orbitals (π orbital of benzene and d_{z^2}) are depopulated. This effect, usually called electron donation, is clearly visible in the negative isosurface. On the other hand, the empty π^* orbitals can also interact with the occupied *d*-band of the metal slab. This effect, usually called back-donation, results in a partial filling of this π^* orbital and a concomitant density increase with a π^* type shape (positive part). To interpret Figure 9, a simulation of these donation and back-donation processes has been performed. First, Figure 10A represents the π ($6b_2$ and $5b_1$) and π^* ($8a_1$ and $4a_2$) orbitals of the isolated benzene molecule distorted as in the bri30 adsorption structure on Pt(111). Second, Figure 10B shows the differential electron density obtained by depopulating arbitrarily the π orbitals and populating the π^* ones in the same proportions. The negative and positive images can easily be compared to the computed exact negative and positive isosurfaces of the differential electron density of Figure 9A, at least for the molecular part: in this region, the two zones inside the cycle and above and between the $C_2-C_3-C_4$ and $C_5-C_6-C_1$ carbon atoms are populated, while the zones outside the cycle, and above and between the $C_1-H_1-C_2-H_2$, C_3-H_3, $C_4-H_4-C_5-H_5$, and C_6-H_6 atoms are depopulated (see Figure 1 for atom numbering). Hence the model of donation from molecule to the surface and back-donation from surface to molecule is validated.

Figure 9 displays also negative and positive differential electron density isosurfaces in the case of adsorption on the hcp0 site on Pt(111). As in the case of the bri30 adsorption, negative figures show a donation effect from π molecular orbitals to metallic atoms, and the positive ones a back-donation from the metal to the π^* molecular orbitals. At the same time, regions between metallic atoms and carbon atoms are populated, which shows the bonding between the molecule and the substrate.

The electron density analysis for the adsorption on Pd(111) and Rh(111) has also been drawn, and it shows the same

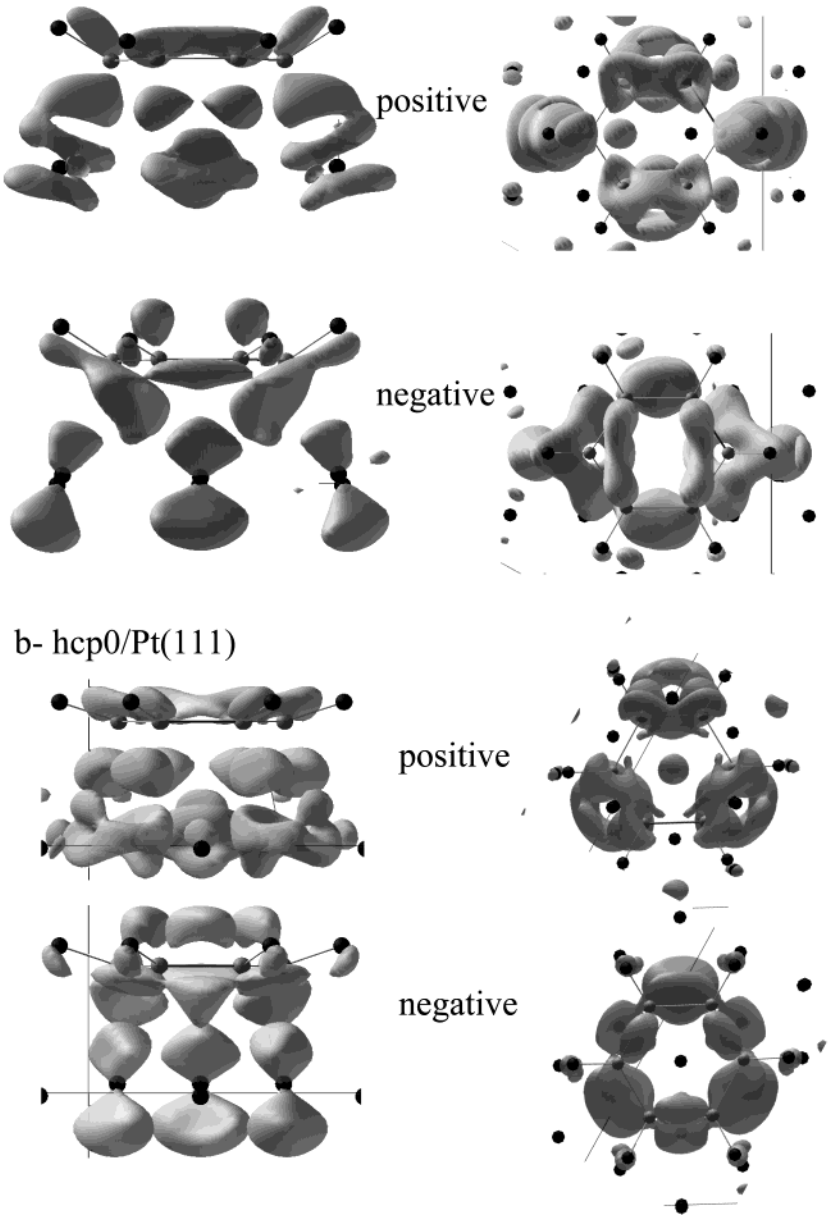

Figure 9. (a) Positive and negative isosurfaces of the differential electron density of benzene adsorbed on bri30 configuration on Pt(111) with respect to the distorted geometries, in a side view (left) and in a top view (right). (b) Same for hcp0 configuration on Pt(111).

donation and back-donation phenomena. Nevertheless, the benzene adsorption on platinum implies a larger variation of charge density than on palladium and rhodium surfaces.

V. Conclusion

In this paper, a quantum chemistry study of the adsorption of benzene, considered as a model aromatic molecule on (111) surfaces of platinum, palladium, and rhodium, is presented. On each surface, four different adsorption possibilities have been studied, two with the aromatic ring bridging two metal atoms (bri), two with the ring bridging three metal atoms (hcp), with an orientation of 0° or 30° angle relative to the metallic rows. In each case, two structures (bri30 and hcp0) are constantly more stable than the other ones.

On Pt(111), the best adsorption geometry for benzene is the bri30 one, with an adsorption energy of −0.90 eV. Calculated vibrational spectra allow one to reproduce the experimental vibrational HREELS spectrum with a very good fit, except for one shoulder, that can be explained by the presence of a small amount of benzene molecule in the hcp0 configuration. This latter configuration is less stable by about 0.23 eV.

On Pd(111), the bri30 structure ($E_{ads} = -1.19$ eV) is still calculated to be more stable than the hcp0 one but only by 0.16 eV. We have performed the vibrational spectra, and their analysis and comparison with the experimental HREELS ones lead us to the conclusion of a coadsorption of benzene in both configurations, with a larger proportion of the bri30 one: a single structure cannot reproduce all the experimental peaks, while the balanced sum of them can. Moreover, the LEED experiments allow us to presume an important role of the coadsorption of benzene with CO, because in this case, only benzene in the hcp0 structure is seen.

On Rh(111), both adsorption structures are calculated with very close adsorption energies (−1.53 and −1.51 eV for bri30 and hcp0, respectively). The combined analysis of the simulated and experimental vibrational spectra leads, as in the case of palladium, to a coadsorption of benzene molecules in both structures. Under this hypothesis, all different peaks and shoulders can be attributed. Moreover, we performed the

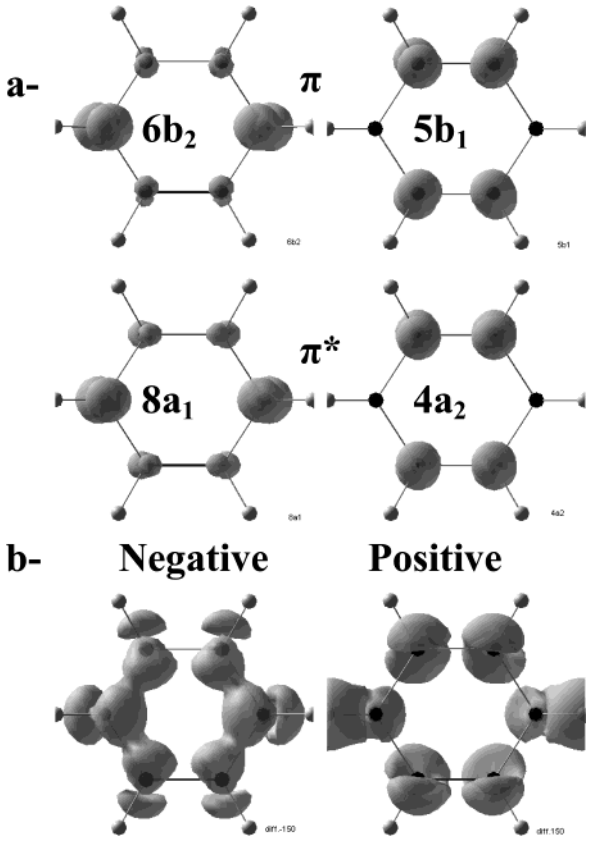

Figure 10. Simulation of the differential electron density images in the case of benzene adsorption on Pt(111) in bri30 configuration (see Figure 1). (a) Representation of the π ($6b_2$ and $5b_1$) and π^* ($8a_1$ and $4a_2$) molecular orbitals of the isolated benzene, distorted as in the bri30 adsorption structure. (b) Simulation of the negative and positive isosurfaces of the charge variation by population of the π^* orbitals and depopulation of the π orbitals.

calculation of coadsorption of benzene with CO, and concluded, as shown experimentally (LEED, STM), that the hcp0 configuration is preferred.

The variation of the adsorption energies on Pt (~ -0.9 eV), Pd (~ -1.2 eV), and Rh (~ -1.5 eV) is explained in terms of geometric distortions and electronic interactions. The adsorption energy is decomposed in three terms: (i) the distortion energy of the molecule, linked to the geometric deformation of the molecule (out-of-plane angles, C−C bond lengths); (ii) the distortion energy of the surface, linked to the distortion of the first metallic layers; and (iii) the interaction energy between the distorted molecule and the distorted surface.

The distortion energies of the molecule and of the surface are both larger for Pt and Rh than for Pd. Moreover, the molecule is significantly more distorted in the bri30 adsorption configuration than in the hcp0 one, while the surface is equivalently distorted in both cases. These distortion energies cannot explain the adsorption energies, larger on Rh than on Pt and Pd, nor the much large adsorption energies in bri30 cases. Hence the interaction energy is the key to understanding these adsorption energies as there is a compromise between distortion and interaction: a strong distortion costs energy but ensures a better interaction between molecule and surface.

An analysis of the projected density of states on molecule and surface atoms and of the differential electron density images allows us to conclude (i) that the interaction is predominantly explained by a donation from molecule to surface and back-donation from surface to molecule, (ii) that the electronic interactions between the π orbitals of the benzene molecule and the *d*-band of the surfaces are better on Rh than on Pt and than on Pd, because of the shape and filling of the metallic *d*-band, and (iii) that the interaction of the molecule with four metal atoms (bri30 configuration) is better than with three metal atoms (hcp configuration). These conclusions help us to understand that the interaction energies are, on one hand, larger in the bri30 than in the hcp0 adsorption case, and, on the other hand, larger for adsorption on Rh than on Pt and on Pd. Finally, the combination of the interaction energies with the distortion energies explains also the relative adsorption energies on Rh, Pt, and Pd, and on bri30 and hcp0 sites.

Quantum chemistry combined with several experimental data can hence help to build a coherent microscopic picture for the adsorption trends of benzene on transition metal surfaces.

Acknowledgment. This work was supported by the Fonds National pour la Science, under program ACI "Surfaces, interfaces et conception de nouveaux matériaux", Project N*o*. S40-01, and the computational center IDRIS (CNRS) under Contract N*o*. 30609.

References and Notes

(1) Sayes, M.; Reyniers, M.-F.; Marin, G. B.; Neurock, M. *J. Phys. Chem. B* **2002**, *106*, 7489.
(2) Sayes, M.; Reyniers, M.-F.; Neurock, M.; Marin, G. B. *J. Phys. Chem. B* **2003**, *107*, 3844.
(3) Cooper, B. H.; Donnis, B. B. L. *Appl. Catal. A Gen.* **1996**, *137*, 203.
(4) Sheppard, N. *Annu. Rev. Phys. Chem.* **1988**, *39*, 589.
(5) Netzer, F. P. *Langmuir* **1991**, *7*, 2544.
(6) Haq, S.; King, D. A. *J. Phys. Chem.* **1996**, *100*, 16957.
(7) Lehwald, S.; Ibach, H.; Demuth, J. E. *Surf. Sci.* **1978**, *78*, 577.
(8) Cemic, F.; Dippel, O.; Hasselbrink, E. *Surf. Sci.* **1995**, *342*, 101.
(9) Wander, A.; Held, G.; Hwang, R. Q.; Blackman, G. S.; Xu, M. L.; de Andres, P.; Van Hove, M. A.; Somorjai, G. A. *Surf. Sci.* **1991**, *249*, 21.
(10) Ogletree, D. F.; Van Hove, M. A.; Somorjai, G. A. *Surf. Sci.* **1987**, *183*, 1.
(11) Weiss, P. S.; Eigler, D. M. *Phys. Rev. Lett.* **1993**, *71*, 3139.
(12) Sautet, P.; Bocquet, M.-L. *Isr. J. Chem.* **1996**, *36*, 63.
(13) Sautet, P.; Bocquet, M.-L. *Phys. Rev. B* **1996**, *53*, 4910.
(14) Sautet, P.; Bocquet, M.-L. *Surf. Sci.* **1994**, *304*, L445.
(15) Tsai, M.-C.; Muetterties, E. L. *J. Am. Chem. Soc.* **1982**, *104*, 2534.
(16) Mate, C. M.; Somorjai, G. A. *Surf. Sci.* **1985**, *160*, 542.
(17) Yau, S.-L.; Kim, Y.-G.; Itaya, K. *J. Am. Chem. Soc.* **1996**, *118*, 7795.
(18) Yimagawa, M.; Fujikawa, T. *Surf. Sci.* **1996**, 357−358, 131.
(19) Somers, J.; Bridge, M. E.; Lloyd, D. R.; McCabe, T. *Surf. Sci.* **1987**, *181*, L167.
(20) Koel, B. E.; Crowell, J. E.; Mate, C. M.; Somorjai, G. A. *J. Phys. Chem.* **1984**, *88*, 1988.
(21) Ohtani, H.; Wilson, R. J.; Chiang, S.; Mate, C. M. *Phys. Rev. Lett.* **1988**, *60*, 2398.
(22) Sautet, P.; Joachim, C. *Chem. Phys. Lett.* **1991**, *185*, 23.
(23) Barbieri, A.; Van Hove, M. A.; Somorjai, G. A. *Surf. Sci.* **1994**, *306*, 261.
(24) Lee, A. F.; Wilson, K.; Lambert, R. M.; Goldoni, A.; Baraldi, A.; Paolucci, G. *J. Phys. Chem. B* **2000**, *104*, 11729.
(25) Waddill, G. D.; Kesmodel, L. L. *Phys. Rev. B* **1985**, *31*, 4940.
(26) Anderson, A. B.; McDevitt, M. R.; Urbach, F. L. *Surf. Sci.* **1984**, *146*, 80.
(27) Garfunkel, E. L.; Minot, C.; Gavezzotti, A.; Simonetta, M. *Surf. Sci.* **1986**, *167*, 177.
(28) Minot, C.; Van Hove, M. A.; Somorjai, G. A. *Surf. Rev. Lett.* **1995**, *3*, 285.
(29) Morin, C.; Simon, D.; Sautet, P. *J. Phys. Chem. B* **2003**, *107*, 2995.
(30) Mittendorfer, F.; Hafner, J. *Surf. Sci.* **2001**, *472*, 133.
(31) Yamagishi, S.; Jenkins, S. J.; King, D. A. *J. Chem. Phys.* **2001**, *114*, 5765.
(32) Kresse, G.; Hafner, J. *Phys. Rev. B* **1993**, *47*, C558.
(33) Kresse, G.; Furthmüller, J. *Comput. Mater. Sci.* **1996**, *6*, 15.

(34) Kresse, G.; Joubert, D. *Phys. Rev. B* **1999**, *59*, 1758.
(35) Perdew, J. P.; Chevary, J. A.; Voslo, S. H.; Jackson, K. A.; Pederson, M. R.; Singh, D. J.; Fiolhais, C. *Phys. Rev. B* **1992**, *46*, 6671.
(36) Monkhorst, H. J.; Pack, J. D. *Phys. Rev. B* **1976**, *13*, 5188.
(37) Methfessel, M.; Paxton, A. *Phys. Rev. B* **1989**, *40*, 3616.
(38) Person, W. B.; Kubulat, K. *J. Mol. Struct.* **1990**, *224*, 225.
(39) Person, W. B.; Zerbi, G. Vibrational Intensities in Infrared and Raman Spectroscopy; Elsevier: Amsterdam, 1982.
(40) Gil, A.; Clotet, A.; Ricart, J. M.; Kresse, G.; García-Hernández, M.; Rösch, N.; Sautet, P. *Surf. Sci.* **2003**, *530*, 71.
(41) Jungwirthova, I.; Kesmodel, L. L. *Surf. Sci.* **2000**, *470*, L39.
(42) Herzberg, G. *Molecular Spectra and Molecular Structure II, Infrared and Raman Spectra of Polyatomic Molecules*; Princeton University Press: 1945, 118.
(43) Ohtani, H.; Van Hove, M. A.; Somorjai, G. A. *J. Phys. Chem.* **1988**, *92*, 3974.
(44) Chou, K. C.; Kim, J.; Baldelli, S.; Somorjai, G. A. *J. Electroan. Chem.* In press.
(45) Koel, B. E.; Crowell, J. E.; Mate, C. M.; Somorjai, G. A. *J. Phys. Chem.* **1984**, *88*, 1988.
(46) Yoon, H. A.; Salmeron, M.; Somorjai, G. A. *Surf. Sci.* **1997**, *373*, 300.
(47) Lin, R. F.; Koestner, R. J.; Van Hove, M. A.; Somorjai, G. A. *Surf. Sci.* **1983**, *134*, 161.
(48) Van Hove, M. A.; Lin, R. F.; Somorjai, G. A. *Phys. Rev. Lett.* **1983**, *51*, 778.
(49) Van Hove, M. A.; Lin, R. F.; Somorjai, G. A. *J. Am. Chem. Soc.* **1986**, *108*, 2532.
(50) Lin, R. F.; Blackman, G. S.; Van Hove, M. A.; Somorjai, G. A. *Acta Crystallogr.* **1987**, *B43*, 368.
(51) Mavrikakis, M.; Rempel, J.; Greeley, J.; Hansen, L. B.; Nørskov, J. K. *J. Chem. Phys.* **2002**, *117*, 6737.
(52) Morin, C.; Eichler, A.; Hirschl, R.; Sautet, P.; Hafner, J. *Surf. Sci.* **2003**, *540*, 474.
(53) Shimanouchi, T. *Tables of Molecular Vibrational Frequencies*; National Bureau of Standards, New York, 1972; Consolidated Vol. 1, pp 1−160.